HAL
open science

A low temperature investigation of the N(2 D) + CH 4 , C 2 H 6 and C 3 H 8 reactions

Dianailys Nuñez-Reyes, Jean-Christophe Loison, Kevin Hickson, Michel Dobrijevic

To cite this version:

Dianailys Nuñez-Reyes, Jean-Christophe Loison, Kevin Hickson, Michel Dobrijevic. A low temperature investigation of the N(2 D) + CH 4 , C 2 H 6 and C 3 H 8 reactions. Physical Chemistry Chemical Physics, 2019, 21 (12), pp.6574-6581. 10.1039/C9CP00798A . hal-02322302

HAL Id: hal-02322302

https://hal.science/hal-02322302v1

Submitted on 11 Jan 2021

HAL is a multi-disciplinary open access archive for the deposit and dissemination of scientific research documents, whether they are published or not. The documents may come from teaching and research institutions in France or abroad, or from public or private research centers.

L'archive ouverte pluridisciplinaire **HAL**, est destinée au dépôt et à la diffusion de documents scientifiques de niveau recherche, publiés ou non, émanant des établissements d'enseignement et de recherche français ou étrangers, des laboratoires publics ou privés.

A low temperature investigation of the $N(^2D) + CH_4$, C_2H_6 and C_3H_8 reactions

Dianailys Nuñez-Reyes,[a,b] Jean-Christophe Loison,[a,b] Kevin M. Hickson,[a,b*] and Michel Dobrijevic[c]

[a]*Université de Bordeaux, Institut des Sciences Moléculaires, UMR 5255, F-33400 Talence, France*
[b]*CNRS, Institut des Sciences Moléculaires ,UMR 5255, F-33400 Talence, France*
[c]*Laboratoire d'Astrophysique de Bordeaux, Université de Bordeaux, CNRS, B18N, allée Geoffroy Saint-Hilaire, F-33615 Pessac, France*

Abstract

The gas-phase reactions between metastable nitrogen atoms, $N(^2D)$ and saturated hydrocarbons CH_4, C_2H_6 and C_3H_8 have been investigated using a supersonic flow reactor over the 296 - 75 K temperature range. $N(^2D)$ was generated as a product of the $C(^3P) + NO \rightarrow N(^2D) + CO$ reaction, with $C(^3P)$ atoms created in-situ by pulsed laser photolysis of CBr_4. The kinetics of $N(^2D)$ loss were followed by vacuum ultraviolet laser induced fluorescence. The measured rate constants for the $N(^2D) + CH_4$ reaction are in good agreement with earlier work and extend the available kinetic data for this process down to 127 K. The measured rate constants for the $N(^2D) + C_2H_6$ and $N(^2D) + C_3H_6$ reactions are in reasonable agreement with previous work at room temperature and extend the available kinetic data for these processes down to 75 K. The rate constants for all three reactions decrease as the temperature falls, indicating the presence of activation barriers for all three processes. While the recommended values for the low temperature rate constants of the $N(^2D) + CH_4$ reaction are close to those reported here, the previous recommendations for the other saturated hydrocarbon reactions significantly overestimate the rate constants for these processes. The effects of the new rate constants on a coupled ion-neutral photochemical model of Titan's atmosphere are discussed.

1 Introduction

Nitrogen is the fifth most abundant element in the Universe behind hydrogen, helium, carbon and oxygen.[1] The reactions of atomic nitrogen are important processes in a wide range of astrochemical environments. In the interstellar medium, N-atoms in their ground electronic ^4S state participate in a series of reactions with other nitrogen containing radicals, effectively controlling the transformation from N to N_2 in dense interstellar clouds.[2, 3] In these regions, the specific form of the major elemental nitrogen reservoir (N or N_2) is critically important for the overall complexity of the molecules present, considering the highly unreactive nature of molecular nitrogen. Excited electronic states of atomic nitrogen, N(^{2}D) and N(^{2}P), play little or no role in the chemistry of the gas-phase interstellar medium as the timescale for radiative relaxation is shorter than the collision timescale. Nevertheless, in contrast to cold interstellar environments, excited state nitrogen atoms participate in the gas-phase chemistry of planetary atmospheres, where large fluxes of energetic photons and high densities lead to numerous collisions with the various atmospheric components. In the Earth's atmosphere, atomic nitrogen is produced through the short wavelength photodissociation of N_2 and through N_2 collisions with photoelectrons in the upper atmosphere.[4] Indeed, the reactions of N(^{4}S) and N(^{2}D) with O_2 are both thought to be major sources of NO in the thermosphere, while subsequent reactions of N(^{4}S) and N(^{2}D) with NO[5, 6] limit the overall odd nitrogen concentration at these altitudes. In Titan's upper atmosphere, both N(^{4}S) and N(^{2}D) atoms are considered to be important reactive species for the formation of nitrogen-bearing compounds. While N(^{4}S) atoms react with radicals such as CH_3,[7] to form nitrogen containing hydrocarbon molecules such as H_2CN (and ultimately HCN),[8] these ground state atoms are largely unreactive with the most abundant closed-shell hydrocarbon molecules present in Titan's atmosphere, CH_4, C_2H_2, C_2H_4 and C_2H_6. Instead, the more reactive metastable N(^{2}D) atoms react with these molecules to form a range of amines, imines and nitriles[9] (N(^{2}P) is much less reactive than N(^{2}D),[10] so that the fate of these atoms is quenching to the ^{2}D state through collisions with N_2, rather than reaction). Although the major reaction channels for the N(^{2}D) + CH_4,[11-15] N(^{2}D) + C_2H_6,[16] N(^{2}D) + C_2H_4 [17, 18] and N(^{2}D) + C_2H_2[19-21] reactions have been identified theoretically and through crossed molecular beam experiments, there are few kinetics measurements of these processes and none at temperatures pertinent to Titan's atmosphere. For the N(^{2}D) + CH_4 reaction, the derived room temperature rate constants[22-25] fall in the range (3.0 – 5.4) × 10^{-12} cm^3 s^{-1}. Black et al.[22] generated N(^{2}D) atoms in their reactor through N_2O photolysis at 147 nm and 123.6 nm. N(^{2}D) removal in the presence of coreagent CH_4 was followed using the chemiluminescent emission from NO($B^2\Pi \rightarrow X^2\Pi$)

produced by the $N(^2D)$ + N_2O reaction. In their study, Fell et al.[23] used a fast flow system where $N(^2D)$ atoms were produced through the microwave discharge of N_2 diluted in He. The $N(^2D)$ concentration was monitored through electron spin resonance spectroscopy. They measured rate constants for $N(^2D)$ removal for numerous coreagent species including CH_4, C_2H_6 and C_3H_8. Umemoto et al.[24] created $N(^2D)$ atoms in their experiments through the multiphoton dissociation of NO at 275.3 nm. These authors detected $N(^2D)$ through two-photon excitation around 269 nm via the $2p^3\ ^2D_{5/2}$ - $2p^23p\ ^2S$ transition. Rapid relaxation to the $2p^23s\ ^2P$ state followed by VUV fluorescence at 149 nm allowed these authors to determine rate constants for the reactions of $N(^2D)$ with various species at room temperature including CH_4, C_2H_6 and C_3H_8. Takayanagi et al.[25] used the pulsed radiolysis – resonance absorption method to perform kinetic measurements over the 292 K- 223 K range, reporting a positive temperature dependence for the $N(^2D)$ + CH_4 reaction, with the rate constant decreasing to a value of $(2.3 \pm 0.2) \times 10^{-12}$ $cm^3\ s^{-1}$ at 223 K. The Arrhenius parameters of A = 4.8×10^{-12} $cm^3\ s^{-1}$ and E/R = 750 recommended by Herron[10] were based on the temperature dependence of the Takayanagi et al.[25] study and the earlier room temperature work (with a correction factor applied to the Fell et al. rate constants - see Herron[10] for further justification). For the $N(^2D)$ + C_2H_6 and $N(^2D)$ + C_3H_8 reactions, kinetic studies have only been performed at room temperature. Fell et al.[23] and Umemoto et al.[24] obtained rate constants of 2.7×10^{-11} $cm^3\ s^{-1}$ and 2.1×10^{-11} $cm^3\ s^{-1}$ for the $N(^2D)$ + C_2H_6 reaction and 4.6×10^{-11} $cm^3\ s^{-1}$ and 3.1×10^{-11} $cm^3\ s^{-1}$ for the $N(^2D)$ + C_3H_8 reaction respectively. The recommended rate constants[10] for these two reactions are 1.9×10^{-11} $cm^3\ s^{-1}$ ($N(^2D)$ + C_2H_6) and 2.9×10^{-11} $cm^3\ s^{-1}$ ($N(^2D)$ + C_3H_8) at 298 K, considering the correction factor of 0.6 that was systematically applied to the Fell et al. results. Given the lack of temperature dependent data, current models of Titan's atmosphere[26, 27] consider temperature independent rate constants for these two processes, equal to the recommended room temperature values.

This study presents kinetic measurements for the $N(^2D)$ + CH_4, C_2H_6 and C_3H_8 reactions down to 75 K using a Laval nozzle supersonic flow reactor. In this work, $N(^2D)$ atoms were generated by chemical reaction, employing the technique described by Nuñez-Reyes & Hickson[6] during their investigation of the $N(^2D)$ + NO reaction. These atoms were detected through on-resonance pulsed laser induced fluorescence in the vacuum ultraviolet wavelength range. The experimental methods are presented in section 2 of the paper. The results are presented and discussed within the context of earlier work in Section 3. Section 4 discusses the astrophysical implications of the present work through an updated photochemical model of Titan's atmosphere. The conclusions are outlined in Section 5.

2 Experimental methods

The experiments performed in this study employed an existing continuous supersonic flow reactor whose main features have been described previously.[28-30]

Further modifications to the apparatus allowing the generation of narrowband tunable radiation in the vacuum ultraviolet wavelength range for the detection of atomic radicals in ground and excited electronic states are reported in later work ($C(^3P)$,[31-33] $H(^2S)$[31, 33-41] and $D(^2S)$, [33, 42] $O(^1D)$,[38, 41, 43-47] and $N(^2D)$).[6] During this work, both Ar and N_2 were used as carrier gases as they result in only slow quenching of $N(^2D)$ atoms.[48, 49] The properties of the Laval nozzles employed in this work are summarized in Table 1.

Table 1 Supersonic flow characteristics

Mach number	1.83± 0.02[a]	1.99 ± 0.03	2.97 ± 0.06
Carrier gas	N_2	Ar	Ar
Density ($\times 10^{16}$ cm^{-3})	9.4 ± 0.2	12.6 ± 0.3	14.7 ± 0.6
Impact pressure (Torr)	8.2 ± 0.1	10.5 ± 0.2	15.3 ± 0.5
Stagnation pressure (Torr)	10.3	13.9	34.9
Temperature (K)	177 ± 2	127 ± 2	75 ± 2
Mean flow velocity (ms^{-1})	496 ± 4	419 ± 3	479 ± 3
Chamber pressure (Torr)	1.4	1.5	1.2

[a] The errors on the Mach number, density, temperature and mean flow velocity (1σ) are calculated from separate measurements of the impact pressure using a Pitot tube as a function of distance from the Laval nozzle and the stagnation pressure within the reservoir.

Room temperature measurements were also performed during the present investigation. These experiments were conducted at reduced flow velocities without a Laval nozzle, to ensure that no pressure gradients existed within the reactor. In a similar manner to the study of Nuñez-Reyes & Hickson,[6] $N(^2D)$ atoms were generated chemically, through the reaction of ground state $C(^3P)$ atoms with nitric oxide

$$C(^3P) + NO \rightarrow N(^2D, {}^4S) + CO \quad (1a)$$

$$\rightarrow O(^3P) + CN \quad (1b)$$

The ratio $[N(^2D) + N(^4S)]/[O(^3P)]$ has been estimated as 1.5 ± 0.3 at room temperature[50] while previous theoretical work predicts that the branching ratio for channel (1a) should decrease by

approximately 50 % between 300 K and 50 K.[51] Ground state C(^{3}P) atoms were produced by the pulsed multiphoton dissociation of carbon tetrabromide, CBr_4, at 266 nm with pulse energies around 26 mJ. C(^{1}D) atoms were also produced during the photolysis process.[31] Possible interferences from secondary reactions are discussed below. To introduce these molecules into the system, a small flow of the carrier gas was diverted into a vessel containing solid CBr_4 at a known fixed (room) temperature and pressure before rejoining the main flow upstream of the Laval nozzle reservoir. The CBr_4 concentration in the flow was estimated to be less than 3.2×10^{13} cm^{-3} as determined by the product of the ratio of the CBr_4 vapour pressure and the total pressure and the flow rate through the vessel $(P_{CBr_4}/P_{vessel}) \times F_{vessel}$. The method employed to follow N(^{2}D) atoms in the present work was on-resonance pulsed laser induced fluorescence in the vacuum ultraviolet range (VUV LIF) via the $2s^22p^3$ $^2D°$ - $2s^22p^2(^3P)3d$ ^2F transition at 116.745 nm. Tunable radiation at and around this wavelength was produced in an identical manner to study of Nuñez-Reyes & Hickson[6] where a more detailed description of the procedure for its generation can be found. The VUV radiation was collimated by a MgF_2 lens at the exit of the tripling cell and steered into the reactor through a 75 cm long sidearm containing baffles to reduce the flux of divergent residual UV radiation. The VUV beam overlapped with the cold supersonic flow at right angles. As the coreagents CH_4, C_2H_6 and C_3H_8 all absorb strongly in the VUV region, this zone was continuously flushed with either N_2 or Ar to minimize the attenuation of the probe beam. The solar blind photomultiplier tube detector (PMT) was placed at right angles to both the probe beam and the supersonic flow, collecting fluorescence from unreacted N(^{2}D) atoms. The PMT was protected from reactive gases within the chamber by a LiF window while the zone separating the PMT from the reactor (containing a LiF lens to focus the VUV light onto the photocathode) was continuously evacuated by a dry pump. As signal levels were small compared with our earlier studies of atomic carbon and oxygen reactions, spurious light sources (residual UV light, scattered VUV light and window fluorescence) were reduced to a minimum, while it was also necessary to connect a preamplifier module to the output of the PMT before signal processing and integration by a boxcar system. Although this provided a substantial improvement in signal-to-noise levels, scattered light and/or window fluorescence from the photolysis laser which could not be entirely removed was also detected. This resulted in saturation of amplified signal for the first 15 microseconds following the photolysis pulse, preventing us from recording VUV LIF signals in this time period throughout the experiments. A delay generator was used to scan the time between photolysis

and probe lasers to obtain the temporal profile of N(^{2}D) atoms. 30 points were recorded at each time point with at least 70 time points recorded for each kinetic profile. Points recorded at negative time delays (that is with the probe laser pulse occurring before the photolysis laser one) allowed the baseline level to be established. Gases (Linde Ar 99.999%, Xe 99.999%, CH_4 99.9995%, C_2H_6 99.5%, C_3H_8 99.5%, Air Liquide N_2 99.999%, NO 99.9%) were used without further purification. Gas cylinders were attached to calibrated mass-flow controllers, allowing the various carrier gas and reagent flows to be regulated precisely.

Potential secondary chemistry

Although several secondary reactions could be occurring in the reactor during these experiments, these are not expected to interfere with the present measurements to any significant extent considering that N(^{2}D) atoms are detected directly. A discussion of the influence of potential secondary reactions has already been provided by Nuñez-Reyes & Hickson[6] for the simpler case of the N(^{2}D) + NO reaction. In the present case, additional secondary processes arising from the reactions of photolysis products C(^{3}P) and C(^{1}D), quenching product N(^{4}S), as well as reaction products CN and O(^{1}D) with the saturated hydrocarbon reagents also need to be considered. Both C(^{3}P) and N(^{4}S) atoms are unreactive with CH_4, C_2H_6 and C_3H_8 at room temperature and below, so that these reactions do not need to be considered further. Although C(^{1}D) will react with all three of these reagents, leading to atomic products such as H(^{2}S) and hydrocarbon radicals such as CH and CH_3,[39, 52] these species will be present in low concentrations and none will yield N(^{2}D) as a product through reaction with NO, the only nitrogen containing excess reagent present in the chamber. Similarly, although the CN and O(^{1}D) products of the C + NO reaction react readily with saturated hydrocarbon molecules,[38, 41, 53] none of these processes are thought to lead to the formation of N(^{2}D) atoms.

3 Results and Discussion

The pseudo-first-order approximation was applied in these experiments, by maintaining both NO and the hydrocarbon reagent C_xH_{2x+2} in excess with respect to both C(^{3}P) and N(^{2}D). Under these conditions, the temporal profile of N(^{2}D) atoms, $I_{\mathrm{N(^2D)}}$, can be described by the following expression

$$I_{\mathrm{N(^2D)}} = \mathrm{C}(\exp(-k'_{\mathrm{a}}t) - \exp(-k'_{\mathrm{b}}t)) \qquad (2)$$

where C is a constant, k'_{a} is the pseudo-first-order rate constant for N(^{2}D) removal, k'_{b} is the pseudo-first-order rate constant for N(^{2}D) production and t is time. The term k'_{a} comprises

several contributions including the pseudo-first-order losses of N(^{2}D) with NO ($k_{N(^2D)+NO}[NO]$), C_xH_{2x+2} ($k_{N(^2D)+C_xH_{2x+2}}[C_xH_{2x+2}]$), any other excess reagent (such as CBr_4 for example ($k_{N(^2D)+CBr_4}[CBr_4]$) and through diffusion ($k_{N(^2D),diff}$). As C(^{3}P) atoms do not react with C_xH_{2x+2}, $k'_b = k_{C(^3P)+NO}[NO] + k_{C(^3P),diff}$. Nevertheless, as the first 15 microseconds of the N(^{2}D) temporal profiles were not exploitable, it was more convenient to use a function of the form

$$I_{N(^2D)} = C\exp(-k'_a t) \qquad (3)$$

to describe the N(^{2}D) signal as a function of time. In this respect, the starting points of individual fits were carefully chosen to avoid the rising part of the temporal profile. Figure 1 shows two profiles of the N(^{2}D) fluorescence intensity as a function of time recorded at 296 K in the presence and absence of C_3H_8.

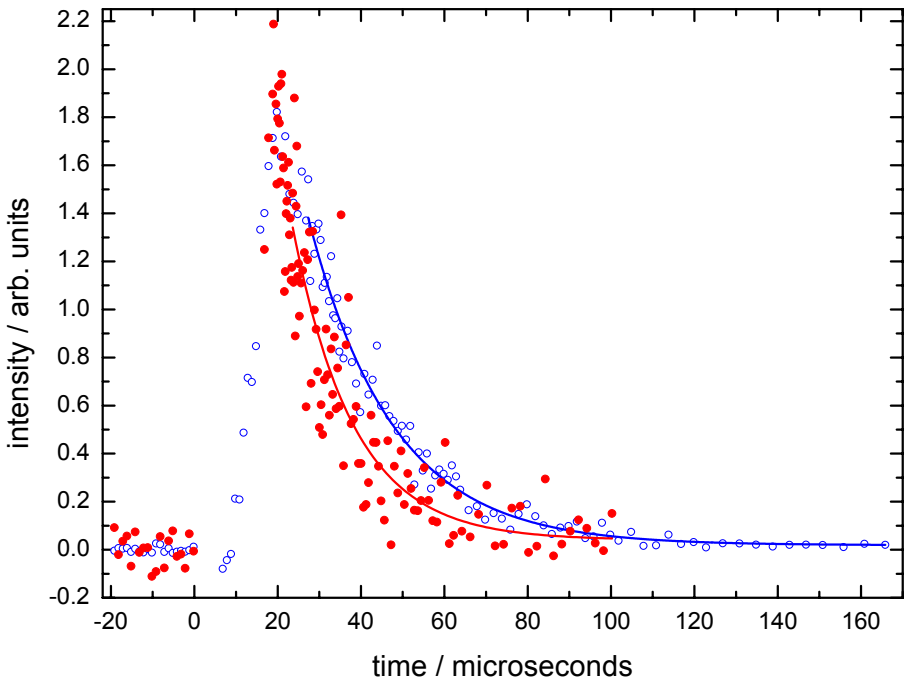

Figure 1 N(^{2}D) VUV LIF intensity as a function time recorded at 296 K. (Red solid circles) without C_3H_8; (blue-solid circles) $[C_3H_8] = 2.3 \times 10^{15}$ cm^{-3}. The signal recorded in the presence of C_3H_8 has been multiplied by an arbitrary factor to allow a comparison of the two traces on the same intensity scale.

Decays similar to those displayed in Figure 1 were recorded at several values of [C_xH_{2x+2}] whilst maintaining a fixed value for [NO]. In this way, any change in the observed decay rate of N(^{2}D) atoms was entirely due to the change in [C_xH_{2x+2}]. Plots of the measured pseudo-first-order rate constant versus [C_xH_{2x+2}] thus yielded the second-order rate constant from weighted linear least-squares fits to the data. The decay curves recorded at high [C_xH_{2x+2}] were always considerably more scattered than the data recorded at low [C_xH_{2x+2}] due to absorption of the N(^{2}D) VUV LIF emission by residual saturated hydrocarbon present in the reactor. Two example second-order plots are shown in Figure 2, for the reactions of N(^{2}D) with CH_4 (purple triangles) and C_2H_6 (red squares) at 177 K.

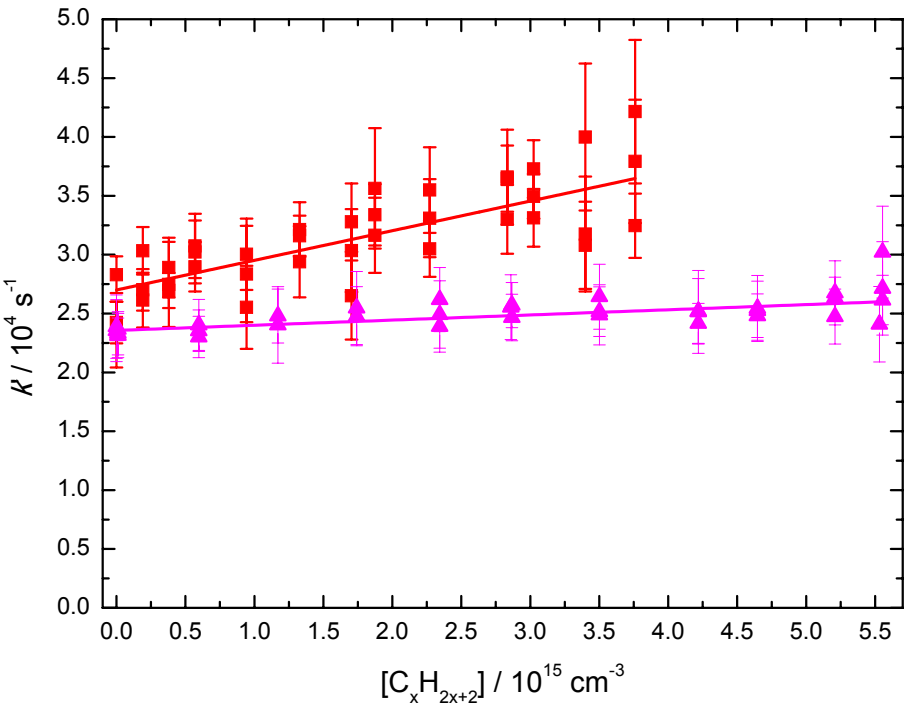

Figure 2 Pseudo-first-order rate constant as a function of saturated hydrocarbon concentration recorded at 177 K. (Red solid squares) the N(^{2}D) + C_2H_6 reaction; (purple solid triangles) the N(^{2}D) + CH_4 reaction. [NO] = 2.7 × 10^{14} cm^{-3}. Solid lines represent weighted linear least-squares fits to the data. The error bars on individual data points (1σ) are derived from exponential fits to temporal profiles such as those displayed in Figure 1.

The y-axis intercept values here correspond to the pseudo-first-order losses of N(^{2}D) through reaction with NO and through diffusion. In these examples, [NO] = 2.7 × 10^{14} cm^{-3} with $k_{\mathrm{N(^2D)+NO}}(177\ \mathrm{K})$ = 8.0 × 10^{-11} cm^3 s^{-1},[6] leading to a theoretical contribution of

approximately 22000 s^{-1} from the $N(^2D)$ + NO reaction and therefore only a minor contribution to the intercept value from diffusional loss of $N(^2D)$ atoms. It is clear from Figure 2 that the rate constant for the $N(^2D)$ + C_2H_6 reaction is substantially faster than the one for the $N(^2D)$ + CH_4 reaction which displays almost no variation over the entire range of $[CH_4]$. The measured rate constants for the $N(^2D)$ + C_xH_{2x+2} reactions are summarized in Table 2 and are displayed in Figure 3 as a function of temperature.

Table 2 Measured rate constants for the $N(^2D)$ + C_xH_{2x+2} reactions

Reaction	T / K	N^a	$[C_xH_{2x+2}]$ / 10^{14} cm^{-3}	[NO] / 10^{14} cm^{-3}	$k_{N(^2D)+C_xH_{2x+2}}$ / 10^{-13} cm^3 s^{-1}
$N(^2D)$ + CH_4	296	44	0 – 46.4	4.3	(24.8 ± 5.4)
	296	24	0 – 45.8	2.2	(21.0 ± 4.3)
	177	34	0 – 55.5	2.6	(4.7 ± 2.4)
	127	20	0 – 61.9	1.6	(1.7 ± 1.5)
$N(^2D)$ + C_2H_6	296	28	0 – 23.6	4.4	(122.0 ± 28.7)
	296	18	0 – 24.4	6.3	(126.4 ± 25.7)
	177	39	0 – 37.6	2.7	(25.2 ± 5.8)
	127	38	0 – 43.2	3.1	(16.8 ± 3.7)
	127	18	0 – 43.1	4.6	(17.6 ± 4.6)
	75	19	0 – 21.3	2.7	(11.1 ± 3.5)
$N(^2D)$ + C_3H_8	296	21	0 – 24.9	6.3	(173.3 ± 37.9)
	177	38	0 – 26.7	2.7	(56.1 ± 12.0)
	127	36	0 – 30.9	3.2	(42.8 ± 9.0)
	127	18	0 – 31.0	4.7	(45.5 ± 9.8)
	75	30	0 – 10.5	2.7	(32.5 ± 8.8)

[a] Number of individual kinetic profiles recorded for each experiment to derive the second-order rate constant.

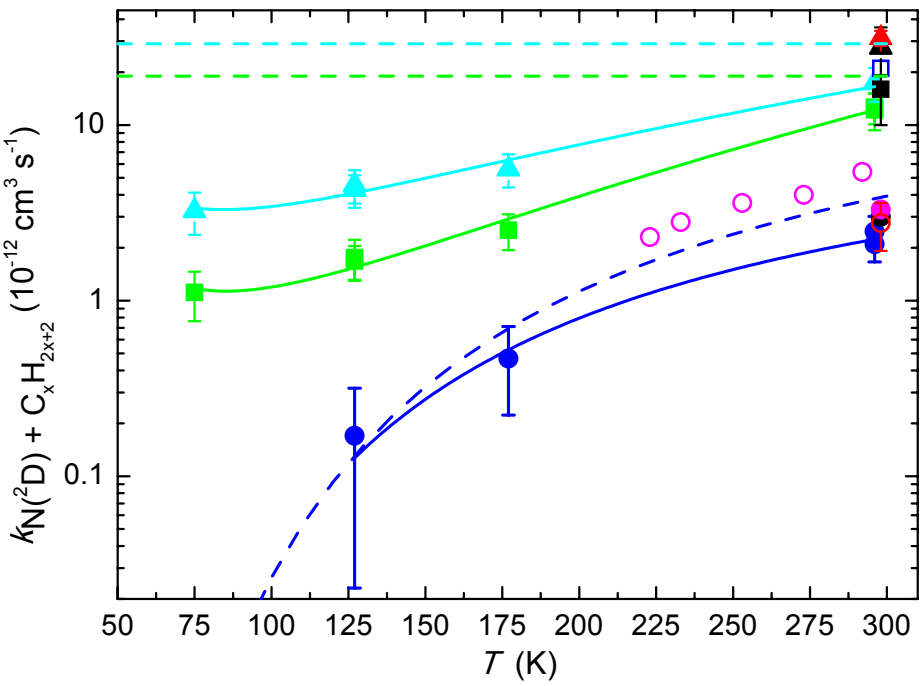

Figure 3. Second order rate constants for the $N(^2D)$ + C_xH_{2x+2} reactions as a function of temperature. The $N(^2D)$ + CH_4 reaction: (Blue solid circles) this work; (purple open circles) (solid black circle) Black et al.[22]; (open red circle) Fell et al.[23]; (solid purple circle) Umemoto et al.[24]; Takayanagi et al.[25] The solid blue lines represent best fits to the present experimental data. The $N(^2D)$ + C_2H_6 reaction: (Green solid squares) this work; (black solid square) Fell et al.[23]; (blue open square) Umemoto et al.[24] The $N(^2D)$ + C_3H_8 reaction: (Cyan solid triangles) this work; (red solid triangle) Fell et al.[23]; (black solid triangle) Umemoto et al.[24] The dashed lines represent the previously recommended values for these reactions. Error bars on the present data represent the combined statistical (1σ) and systematic errors (estimated to be 20 % of the nominal value of the rate constant except for measurements of the $N(^2D)$ + CH_4 reaction at 177 K and 127 K where it was estimated to be 50 %).

The $N(^2D)$ + CH_4 reaction At room temperature, experiments were performed with two different NO concentrations (2.2×10^{14} cm^{-3} and 4.3×10^{14} cm^{-3}) to test for the influence of potential secondary reactions, yielding similar values for $k_{N(^2D)+CH_4}$(296 K) = $(2.1 \pm 0.4) \times 10^{-12}$ cm^3 s^{-1} and $(2.5 \pm 0.5) \times 10^{-12}$ cm^3 s^{-1}. These values are slightly lower than those obtained by previous studies[22-25] with values in the range $(3.0 - 5.4) \times 10^{-12}$ cm^3 s^{-1}. The measured rate constants for the $N(^2D)$ + CH_4 reaction below room temperature are slower

than 10^{-12} cm^{-3} s^{-1}; a value which is normally considered as the lower limit for rate constant measurements through the Laval nozzle method (assuming that the minor reagent decay can be followed over at least two half-lives). If we consider the measurements performed at 177 K as an example, the nozzle used has a characteristic hydrodynamic time of ~250 microseconds (that is, the time over which the nominal characteristics of the supersonic flow are valid). In this case, the maximum [CH_4] used in these experiments was 5.6×10^{15} cm^{-3} which constitutes approximately 6 % of the total flow, and therefore approaching the upper limit for the added coreagent concentration before significant deviations from the nominal flow conditions occur (N_2 carrier gas density = 9.4×10^{16} cm^{-3}). The measured rate constant for the N(^{2}D) + CH_4 reaction at 177 K is 4.7×10^{-13} cm^3 s^{-1} allowing us to calculate a half-life time, $t_{1/2} = (\ln(2)/k') = 260$ microseconds. Consequently, the loss of N(^{2}D) due to the N(^{2}D) + CH_4 reaction alone over the entire duration of the flow at 177 K is significantly less than the loss due to the competing N(^{2}D) + NO reaction ($t_{1/2}$ = 29 microseconds). Although a clear progression of the pseudo-first-order rate constant as a function of [CH_4] is obtained in these experiments (see Figure 2), it is important to realize that the derived second-order rate constants at 177 K and at 127 K are characterized by substantially larger uncertainties than usually associated with this type of measurement. In this respect, we have increased our estimate of the systematic errors on these two measurements to 50 % of the nominal value, although an upper limit value of 3.2×10^{-13} cm^3 s^{-1} could also be considered as appropriate for the measured rate constant at 127 K. Nevertheless, the measured rate constants are in reasonably good agreement with the recommended ones.[10] Indeed, the recommended Arrhenius parameters A = 4.8×10^{-11} cm^3 s^{-1} and (Ea/R) = 750 K yield $k_{N(^2D)+CH_4}$(177 K) = 6.9×10^{-13} cm^3 s^{-1} and $k_{N(^2D)+CH_4}$(127 K) = 1.3×10^{-13} cm^3 s^{-1} which are close to the values obtained in this work ($k_{N(^2D)+CH_4}$(177 K) = $(4.7 \pm 2.4) \times 10^{-13}$ cm^3 s^{-1} and $k_{N(^2D)+CH_4}$(127 K) = $(1.7 \pm 1.5) \times 10^{-13}$ cm^3 s^{-1}). An Arrhenius fit to the present data yields the following Arrhenius parameters; A = 1.93×10^{-11} cm^3 s^{-1} and (Ea/R) = 638 K. Given the slow rate constants at 177 K and 127 K, no attempt was made to measure rate constants at lower temperature.

The N(^{2}D) + C_2H_6 reaction In a similar manner to the N(^{2}D) + CH_4 reaction, experiments were performed with two different NO concentrations (4.4×10^{14} cm^{-3} and 6.6×10^{14} cm^{-3}) to test for the influence of potential secondary reactions, yielding similar values for $k_{N(^2D)+C_2H_6}$(296 K) = $(1.2 \pm 0.3) \times 10^{-11}$ cm^3 s^{-1} and $(1.3 \pm 0.3) \times 10^{-11}$ cm^3 s^{-1}. These values are slightly lower than previous work by Fell et al.[23] and Umemoto et al.[24] which yielded

values of (1.6 ± 0.6) × 10^{-11} cm^3 s^{-1} (corrected value – see Herron[10] for more detail) and (2.1 ± 0.2) × 10^{-11} cm^3 s^{-1} respectively. The rate constant is seen to decrease as the temperature falls, reaching a value of (1.1 ± 0.3) × 10^{-12} cm^3 s^{-1} at 75 K. An Arrhenius fit to the present data does not provide an adequate description of the rate constant over the entire temperature range, so we choose instead to use a modified Arrhenius type expression ($k = A \times (T/300)^n \times \exp(-Ea/RT)$) where A = 3.58 × 10^{-12} cm^3 s^{-1}, n = 4.45 and (Ea/R) = -379 K. These parameters are valid over the 75 – 296 K temperature range. The deviation from Arrhenius behavior at low temperature might be an indication that H atom tunneling plays a small but non-negligible role in the $N(^2D)$ + C_2H_6 reaction. Interestingly, photochemical models of Titan's atmosphere[26, 27] use the recommended room temperature rate constant[10] $k_{N(^2D)+C_2H_6}$ = 1.9 × 10^{-11} cm^3 s^{-1} as a temperature independent value to describe the reactivity of the $N(^2D)$ + C_2H_6 reaction at lower temperature. At temperatures relevant to Titan's atmosphere (taking 150 K as a representative temperature) the fit to the present data yields a rate constant of 2.1 × 10^{-12} cm^3 s^{-1}; almost an order of magnitude lower than the currently recommended value. Following the joint experimental and theoretical study of this reaction by Balucani et al.[16] the major products are expected to be methanimine (CH_2NH) and CH_3 with small contributions from ethanimine (CH_3CH_2NH) and H atoms, NH and C_2H_5, as well as other products at the 1 % level or less.

The $N(^2D)$ + C_3H_8 reaction The measured rate constants at 296 K were found to be lower than the values obtained previously by Fell et al.[23] and Umemoto et al.[24] of (2.8 ± 0.8) × 10^{-11} cm^3 s^{-1} (corrected value) and (3.1 ± 0.3) × 10^{-11} cm^3 s^{-1} respectively. Given the discrepancy between the present and previous studies, further tests were performed to check for potential errors in the current work. In particular, as $N(^2D)$ atoms are formed through reaction (1a) rather than prompt formation through direct photolysis, it is possible that $N(^2D)$ formation and $N(^2D)$ loss through the $N(^2D)$ + C_3H_8 reaction were occurring over the same time period. Indeed, such an effect is expected to lead to slower pseudo-first-order rate constants for the target reaction. During these test experiments, pseudo-first-order rate constants for the $N(^2D)$ + C_3H_8 reaction were measured with three different fixed NO concentrations (2.2, 4.2 and 6.3 × 10^{14} cm^{-3}) at room temperature. Assuming a rate constant of 1.5 × 10^{-10} cm^3 s^{-1} for reaction (1),[54] we obtain pseudo-first-order rate constants of 3.4, 6.3, 9.4 × 10^4 s^{-1} respectively thus allowing us to calculate the half-life times for $N(^2D)$ formation under these conditions. The delay times when only 13 % of the initial $C(^3P)$ remains to be converted to $N(^2D)$ (corresponding to three half-lives) are 64, 33 and 22 μs, indicating that data acquired at delays

shorter than these values may not accurately reflect the kinetics of the $N(^2D) + C_3H_8$ reaction. For the lowest NO concentration, the data acquired after 64 μs was difficult to analyse given the weak signal levels, with a measured rate constant of $(1.2 \pm 0.2) \times 10^{-11}$ cm^3 s^{-1}. With the intermediate NO concentration, a similar measured rate constant of $(1.2 \pm 0.2) \times 10^{-11}$ cm^3 s^{-1} was obtained. Only the rate constant value obtained for the $N(^2D) + C_3H_8$ reaction with [NO] = 6.3×10^{14} cm^{-3} (yielding $k_{N(^2D)+C_3H_8}$(296 K) = $(1.7 \pm 0.4) \times 10^{-11}$ cm^3 s^{-1} respectively) was retained to derive the temperature dependent fitting parameters. The rate constant decreases as the temperature falls reaching a value of $(3.2 \pm 0.9) \times 10^{-12}$ cm^3 s^{-1} at 75 K. As the Arrhenius expression does not yield a good fit to the data over the entire temperature range, the modified Arrhenius type expression described above is used instead, where A = 7.36×10^{-12} cm^3 s^{-1}, n = 2.99 and (Ea/R) = -252 K. These parameters are valid over the 75 – 296 K temperature range. Current photochemical models of Titan's atmosphere[26, 27] use the recommended room temperature rate constant[10] $k_{N(^2D)+C_3H_8}$ = 2.9×10^{-11} cm^3 s^{-1} as a temperature independent value to describe the reactivity of the $N(^2D) + C_3H_8$ reaction. At 150 K, the fit to the present data predicts a rate constant of 5.0×10^{-12} cm^3 s^{-1}; six times smaller than the currently recommended value.

4 Influence of the new rate constants on Titan's atmospheric chemistry

We wanted to test the effect of the new rate constants on current models of Titan's atmosphere. To do this, we employed the 1D-photochemical model described by Dobrijevic et al.[26] with more recent updates related to the chemistry of aromatic compounds,[55] although a detailed description is not provided here (see Dobrijevic et al.[26]). This model treats the coupled chemistry of neutral and ionic species (both cations and anions) to provide an accurate description of the chemistry occurring from the lower atmosphere all the way up to the ionosphere, including high resolution absorption cross-sections for an improved description of N_2 photodissociation. Earlier models by these authors which did not include ions already updated the neutral chemistry of nitrogen bearing molecules.[8, 9, 56] Indeed, an uncertainty propagation study by Loison et al.[9] focusing on the chemistry of nitriles, amines and imines clearly identified the $N(^2D) + CH_4$ and $N(^2D) + C_2H_6$ reactions as key reactions for future study in order to improve the accuracy of model predictions.

Here, we ran two different simulations to examine the effects of the measured rate constants on the species mole fractions as a function of altitude. The first employed the previously recommended rate constants and branching ratios for the $N(^2D) + CH_4$, C_2H_6 and C_3H_8

reactions to yield the standard profiles. The second used the new values as described by the Arrhenius parameters for the respective reactions as presented in section 3. As we do not measure the various product channels for these processes, the relative branching ratios remain unchanged. The differences produced by the two models for various species at 1000 km are summarized in Table 3.

Table 3 Mole fractions at 1000 km produced by the two model runs.

Species	Mole fraction (New Model)	Difference (with respect to the standard model) / %
C_2H_6	2.3×10^{-5}	+9.3
C_3H_8	3.45×10^{-7}	+9.4
C_4N_2	8.3×10^{-7}	+9.4
NH_2	8.7×10^{-7}	-10.8
NH_3	8.6×10^{-7}	-10.6
CH_2NH	1.75×10^{-5}	-11.1
CH_3NH_2	9.35×10^{-10}	-10.6

Due to the low mole fraction of C_3H_8 in Titan's atmosphere, the reaction of $N(^2D)$ with C_3H_8 has a negligible influence on the chemistry in both models. For the other two reactions, the new rate constants lead to only small differences in the mole fraction profiles for all species at altitudes which correspond to the peak of the $N(^2D)$ mole fraction profile. Taking CH_2NH as an example, this species is a major product of the $N(^2D) + CH_4$ reaction with the channel leading to $CH_2NH + H$ considered to represent 80 % of the total, while the products $CH_3 + CH_2NH$ are considered to be the sole products of the $N(^2D) + C_2H_6$ reaction in current models. By examining the integrated column rates, we note that the $N(^2D) + CH_4$ reaction represents the major source of CH_2NH in the standard model (47 %), followed by the $NH + CH_3 \rightarrow CH_2NH + H$ (30 %) and $CH_2NH_2^+ + e^-$ reactions (although $CH_2NH_2^+$ is almost entirely formed by proton transfer reactions with CH_2NH, so this mostly just recycles between CH_2NH and $CH_2NH_2^+$ with only a minor loss channel to form $NH_2 + {}^3CH_2$). This result also holds for the new model given the very minor change in the rate constant values for the $N(^2D) + CH_4$ reaction between the two simulations. In the standard model, the $N(^2D) + C_2H_6$ reaction represents the third largest source of CH_2NH in Titan's atmosphere, albeit with a contribution of only 2.5 % due to the relatively low mole fraction of C_2H_6 with respect to CH_4

(and despite the much larger rate constant). After the new rate constant is included, the $N(^2D)$ + C_2H_6 reaction becomes an entirely negligible source of CH_2NH (0.3 %), with a decrease of the integrated rate by a factor of 8 between the two models.

As CH_3NH_2 is formed through the NH_2 + CH_3 reaction, this species also decreases slightly in the new model due to the less efficient $CH_2NH_2^+$ + e^- dissociative recombination reaction where NH_2 is a minor reaction product as described above. Similarly, the NH_3 mole fraction also decreases as it forms mostly from reactions of NH_2.

The $N(^2D)$ + CH_4 reaction remains the major loss process for $N(^2D)$ atoms in the atmosphere of Titan representing approximately 28 % of the total $N(^2D)$ removal, followed by the $N(^2D)$ + HCN (22 %) and $N(^2D)$ + C_2H_2 (13 %) reactions. Whereas the $N(^2D)$ + C_2H_6 reaction was the 9th most important loss process for $N(^2D)$ (representing approximately 1% of its total removal), with the new rate constants it now represents only 0.1 % of $N(^2D)$ loss.

While the new model results are similar to those of the standard model, it will be interesting to test the effects of the new and more realistic error bars for these reactions on the mole fraction profiles of a range of atmospheric species obtained through uncertainty propagation studies. Previous models (see Loison et al.[55] for example) employed values for the uncertainty factor, F = 1.5 for the $N(^2D)$ + C_2H_6, C_3H_8 reactions. In light of the present experimental results, it is clear that these uncertainties were severely underestimated. While these findings illustrate the difficulty of attributing realistic uncertainties to reactions that have only been investigated at temperatures far from the relevant range, they also reinforce the need for kinetic measurements at appropriate temperatures. Indeed, even though the measured rate constants for the $N(^2D)$ + CH_4 reaction are close to the previously recommended ones, the new uncertainties associated to this process might lead to an entirely different set of key reactions compared to earlier work. As further experimental studies of other important $N(^2D)$ reactions are currently underway, a more detailed uncertainty propagation study will be performed at a later date once their rate constants and associated uncertainties have been fully characterized.

5 Conclusions

Here we present a temperature dependent kinetic study of the reactions of metastable nitrogen atoms in the ^2D state with the saturated hydrocarbons CH_4, C_2H_6 and C_3H_8. A supersonic flow (Laval nozzle) reactor was used to perform these measurements at temperatures as low as 75 K. As $N(^2D)$ atoms are difficult to generate photolytically, a chemical source of these atoms was employed, through the reaction of $C(^3P)$ atoms with NO molecules as first described by

Nuñez-Reyes & Hickson.[6] $C(^3P)$ atoms themselves were produced by the multiphoton dissociation of CBr_4 molecules, while $N(^2D)$ atoms were detected directly through vacuum ultraviolet laser induced fluorescence. While the measured rate constants for the $N(^2D) + CH_4$ reaction are in good agreement with earlier work at higher temperature, the values derived for the $N(^2D) + C_2H_6$ and $N(^2D) + C_3H_8$ reactions are significantly smaller at low temperature than previous estimates based on earlier room temperature results. The effects of the new rate constants are tested on a coupled ion-neutral photochemical model of Titan's atmosphere. These simulations confirm that the $N(^2D) + CH_4$ reaction is the main loss process for $N(^2D)$ atoms in Titan's atmosphere in addition to being the major source of CH_2NH. In contrast, the $N(^2D) + C_2H_6$ and $N(^2D) + C_3H_8$ reactions are shown to be negligibly important processes in the overall photochemistry of Titan's atmosphere. The need for uncertainty propagation studies to test the effects of the new rate constant uncertainties, alongside those of future measurements, is highlighted.

Acknowledgements

K.M.H. and D.N.R acknowledge support from the French program ''Physique et Chimie du Milieu Interstellaire" (PCMI) of the CNRS/INSU with the INC/INP co-funded by the CEA and CNES as well as preliminary funding from the "Program National de Planétologie" (PNP) of the CNRS/INSU.

References

1. E. B. Jenkins, *Astrophys. J.*, 2009, **700**, 1299-1348.
2. J. Daranlot, M. Jorfi, C. Xie, A. Bergeat, M. Costes, P. Caubet, D. Xie, H. Guo, P. Honvault and K. M. Hickson, *Science*, 2011, **334**, 1538-1541.
3. J. Daranlot, U. Hincelin, A. Bergeat, M. Costes, J. C. Loison, V. Wakelam and K. M. Hickson, *Proc. Natl. Acad. Sci. U. S. A.*, 2012, **109**, 10233-10238.
4. J.-C. Gérard, *Planet. Space Sci.*, 1992, **40**, 337-353.
5. P. O. Wennberg, J. G. Anderson and D. K. Weisenstein, *J. Geophys. Res.: Atmos.*, 1994, **99**, 18839-18846.
6. D. Nuñez-Reyes and K. M. Hickson, *Phys. Chem. Chem. Phys.*, 2018, **20**, 17442-17447.
7. G. Marston, F. L. Nesbitt, D. F. Nava, W. A. Payne and L. J. Stief, *J. Phys. Chem*, 1989, **93**, 5769-5774.
8. E. Hébrard, M. Dobrijevic, J. C. Loison, A. Bergeat and K. M. Hickson, *Astron. Astrophys.*, 2012, **541**, A21.
9. J. C. Loison, E. Hébrard, M. Dobrijevic, K. M. Hickson, F. Caralp, V. Hue, G. Gronoff, O. Venot and Y. Bénilan, *Icarus*, 2015, **247**, 218-247.
10. J. T. Herron, *J. Phys. Chem. Ref. Data*, 1999, **28**, 1453-1483.
11. N. Balucani, A. Bergeat, L. Cartechini, G. G. Volpi, P. Casavecchia, D. Skouteris and M. Rosi, *J. Phys. Chem. A*, 2009, **113**, 11138-11152.

12. C.-M. Ouk, N. Zvereva-Loëte and B. Bussery-Honvault, *Chem. Phys. Lett.*, 2011, **515**, 13-18.
13. C.-M. Ouk, N. Zvereva-Loëte, Y. Scribano and B. Bussery-Honvault, *J. Comput. Chem.*, 2012, **33**, 2211-2224.
14. M. Rosi, S. Falcinelli, N. Balucani, P. Casavecchia, F. Leonori and D. Skouteris, in Computational Science and Its Applications – ICCSA 2012, ed. B. Murgante, O. Gervasi, S. Misra, et al., Lecture Notes in Computer Science, Springer, Berlin Heidelberg, 2013, vol. 7333, p. 331-344.
15. M. Rosi, S. Falcinelli, N. Balucani, P. Casavecchia and D. Skouteris, in Computational Science and Its Applications – ICCSA 2013, ed. B. Murgante, S. Misra, M. Carlini, et al., Lecture Notes in Computer Science, Springer, Berlin Heidelberg, 2013, vol. 7971, p. 47-56.
16. N. Balucani, F. Leonori, R. Petrucci, M. Stazi, D. Skouteris, M. Rosi and P. Casavecchia, *Faraday Discuss.*, 2010, **147**, 189-216.
17. N. Balucani, D. Skouteris, F. Leonori, R. Petrucci, M. Hamberg, W. D. Geppert, P. Casavecchia and M. Rosi, *J. Phys. Chem. A*, 2012, **116**, 10467-10479.
18. N. Balucani, L. Cartechini, M. Alagia, P. Casavecchia and G. G. Volpi, *J. Phys. Chem. A*, 2000, **104**, 5655-5659.
19. N. Balucani, M. Alagia, L. Cartechini, P. Casavecchia, G. G. Volpi, K. Sato, T. Takayanagi and Y. Kurosaki, *J. Am. Chem. Soc.*, 2000, **122**, 4443-4450.
20. T. Takayanagi, Y. Kurosaki, K. Misawa, M. Sugiura, Y. Kobayashi, K. Sato and S. Tsunashima, *J. Phys. Chem. A*, 1998, **102**, 6251-6258.
21. T. Takayanagi, Y. Kurosaki, K. Yokoyama, K. Sato and S. Tsunashima, *Chem. Phys. Lett.*, 1999, **312**, 503-510.
22. G. Black, T. G. Slanger, G. A. St. John and R. A. Young, *J. Chem. Phys.*, 1969, **51**, 116-121.
23. B. Fell, I. V. Rivas and D. L. McFadden, *J. Phys. Chem*, 1981, **85**, 224-228.
24. H. Umemoto, N. Hachiya, E. Matsunaga, A. Suda and M. Kawasaki, *Chem. Phys. Lett.*, 1998, **296**, 203-207.
25. T. Takayanagi, Y. Kurosaki, K. Sato, K. Misawa, Y. Kobayashi and S. Tsunashima, *J. Phys. Chem. A*, 1999, **103**, 250-255.
26. M. Dobrijevic, J. C. Loison, K. M. Hickson and G. Gronoff, *Icarus*, 2016, **268**, 313-339.
27. V. Vuitton, R. V. Yelle, S. J. Klippenstein, S. M. Hörst and P. Lavvas, *Icarus*, 2018, DOI: https://doi.org/10.1016/j.icarus.2018.06.013.
28. N. Daugey, P. Caubet, B. Retail, M. Costes, A. Bergeat and G. Dorthe, *Phys. Chem. Chem. Phys.*, 2005, **7**, 2921-2927.
29. N. Daugey, P. Caubet, A. Bergeat, M. Costes and K. M. Hickson, *Phys. Chem. Chem. Phys.*, 2008, **10**, 729-737.
30. J. Daranlot, A. Bergeat, F. Caralp, P. Caubet, M. Costes, W. Forst, J. C. Loison and K. M. Hickson, *Chemphyschem*, 2010, **11**, 4002-4010.
31. R. J. Shannon, C. Cossou, J.-C. Loison, P. Caubet, N. Balucani, P. W. Seakins, V. Wakelam and K. M. Hickson, *RSC Adv.*, 2014, **4**, 26342-26353.
32. K. Hickson, M., J.-C. Loison, J. Bourgalais, M. Capron, S. Le Picard, D., F. Goulay and V. Wakelam, *Astrophys. J.*, 2015, **812**, 107.
33. K. M. Hickson, J.-C. Loison, D. Nuñez-Reyes and R. Méreau, *J. Phys. Chem. Lett.*, 2016, **7**, 3641-3646.
34. J. Bourgalais, M. Capron, R. K. A. Kailasanathan, D. L. Osborn, K. M. Hickson, J.-C. Loison, V. Wakelam, F. Goulay and S. D. Le Picard, *Astrophys. J.*, 2015, **812**, 106.

35. K. M. Hickson, J.-C. Loison, H. Guo and Y. V. Suleimanov, *J. Phys. Chem. Lett.*, 2015, **6**, 4194-4199.
36. K. M. Hickson, J.-C. Loison, F. Lique and J. Kłos, *J. Phys. Chem. A*, 2016, **120**, 2504-2513.
37. K. M. Hickson, J.-C. Loison and V. Wakelam, *Chem. Phys. Lett.*, 2016, **659**, 70-75.
38. Q. Y. Meng, K. M. Hickson, K. J. Shao, J. C. Loisonc and D. H. Zhang, *Phys. Chem. Chem. Phys.*, 2016, **18**, 29286-29292.
39. D. Nuñez-Reyes and K. M. Hickson, *J. Phys. Chem. A*, 2017, **121**, 3851-3857.
40. D. Nuñez-Reyes and K. M. Hickson, *Chem. Phys. Lett.*, 2017, **687**, 330-335.
41. D. Nuñez-Reyes and K. M. Hickson, *J. Phys. Chem. A*, 2018, **122**, 4696-4703.
42. K. M. Hickson and Y. V. Suleimanov, *Phys. Chem. Chem. Phys.*, 2017, **19**, 480-486.
43. R. Grondin, J.-C. Loison and K. M. Hickson, *J. Phys. Chem. A*, 2016, **120**, 4838-4844.
44. K. M. Hickson and Y. V. Suleimanov, *J. Phys. Chem. A*, 2017, **121**, 1916-1923.
45. D. Nuñez-Reyes, K. M. Hickson, P. Larrégaray, L. Bonnet, T. González-Lezana and Y. V. Suleimanov, *Phys. Chem. Chem. Phys.*, 2018, **20**, 4404-4414.
46. D. Nuñez-Reyes, J. Kłos, M. H. Alexander, P. J. Dagdigian and K. M. Hickson, *J. Chem. Phys.*, 2018, **148**, 124311.
47. D. Nuñez-Reyes and K. M. Hickson, *J. Phys. Chem. A*, 2018, **122**, 4002-4008.
48. T. Suzuki, Y. Shihira, T. Sato, H. Umemoto and S. Tsunashima, *J. Chem. Soc., Faraday Trans*, 1993, **89**, 995-999.
49. C. L. Lin and F. Kaufman, *J. Chem. Phys.*, 1971, **55**, 3760-3770.
50. A. Bergeat, T. Calvo, G. Dorthe and J.-C. Loison, *Chem. Phys. Lett.*, 1999, **308**, 7-12.
51. S. Andersson, N. Markovic and G. Nyman, *J. Phys. Chem A.*, 2003, **107**, 5439-5447.
52. F. Leonori, D. Skouteris, R. Petrucci, P. Casavecchia, M. Rosi and N. Balucani, *J. Chem. Phys.*, 2013, **138**, 024311.
53. I. R. Sims, J. L. Queffelec, D. Travers, B. R. Rowe, L. B. Herbert, J. Karthauser and I. W. M. Smith, *Chem. Phys. Lett.*, 1993, **211**, 461-468.
54. W. D. Geppert, D. Reignier, T. Stoecklin, C. Naulin, M. Costes, D. Chastaing, S. D. Le Picard, I. R. Sims and I. W. M. Smith, *Phys. Chem. Chem. Phys.*, 2000, **2**, 2873-2881.
55. J. C. Loison, M. Dobrijevic and K. M. Hickson, *Icarus,* submitted.
56. M. Dobrijevic, E. Hébrard, J. C. Loison and K. M. Hickson, *Icarus*, 2014, **228**, 324-346.

One sentence summary for TOC entry:

Low temperature rate constants for the $N(^2D)$ + C_2H_6, C_3H_8 reactions are shown to be much smaller than previously thought.